Analysis of microinductor performance in a 20-100 Mhz DC/DC converter

Analysis of Microinductor Performance in a 20–100 MHz DC/DC Converter

Ronan Meere, *Student Member, IEEE*, Terence O'Donnell, *Member, IEEE*, Henk Jan Bergveld, Ningning Wang, and Seán Cian O'Mathuna

***Abstract*—This paper presents a low-profile thin-film microfabricated inductor on silicon and its performance in a high-frequency low-power dc/dc converter. The design of the inductors has focused on maximizing efficiency while maintaining a relatively flat frequency response up to 30 MHz. The inductance at 20 MHz is approximately 150 nH with a resistance of 1.8 Ω. The performance of the microinductor has been compared to two conventional commercially available 150-nH chip inductors. One of the chip inductors has a magnetic-material core and the other is an air core. The maximum efficiency of the microinductor, which relates the power loss of the microinductor to output power loss of the converter, is measured to be approximately 93% at 20 MHz. The low-power dc/dc converter operates in the tens of milliwatts output power range, with an input voltage of 1.8 V and an output voltage programmable between 0 and 1.8 V. The converter maximum efficiency when using the microinductor on silicon is 78.5% at 20 MHz, which is approximately 2% lower than the efficiency using the conventional chip inductors.**

***Index Terms*—DC/DC conversion, high frequency, low profile, magnetic-core inductors.**

I. Introduction

THE INCREASE in functionality and size reduction of portable electronic products is driving the requirement for miniaturization and integration of low-power dc/dc converters. The integration of the passive components has so far retarded progress toward monolithic integration of the converter. Passive component integration has been difficult due to the fact that high converter switching frequencies are required to reduce passive values, and hence size, to the point where integration on-chip or in-package becomes feasible. However, with the advances in semiconductor technology, the implementation of high-efficiency, high-frequency active devices has become feasible. For example, recent research activities within several semiconductor companies have suggested that dc/dc down-converter switching frequency may be increased to tens or even hundreds of megahertzs [1]–[3].

Manuscript received December 19, 2008; revised March 29, 2009. Current version published August 28, 2009. This work was supported by the Enterprise Ireland under the Industry Led Research Programme ILRP/PEIG/05. Recommended for publication by Associate Editor S. Y. (Ron) Hui.

R. Meere, T. O'Donnell, N. Wang, and S. C. O'Mathuna are with the Microsystems Centre, Tyndall National Institute, University College Cork, Cork 353, Ireland (e-mail: ronan.meere@tyndall.ie).

H. J. Bergveld is with NXP Semiconductors, Corporate Innovation and Technology, Research, High Tech Campus 32, 5656 AE, Eindhoven, The Netherlands (e-mail: henkjan.bergveld@nxp.com).

Color versions of one or more of the figures in this paper are available online at http://ieeexplore.ieee.org.

Digital Object Identifier 10.1109/TPEL.2009.2021942

TABLE I
State of the Art of MicroInductor Technology Implemented in a DC/DC Converter

Author	Freq (MHz)	L (μH)	Conv. Eff.	Inductor Area
Kowase '05	1.0	0.14	80.0%	225 mm^2
Kim '01	1.2	1.6	80.0%	78 mm^2
Kim '02	1.8	1	81.0%	25 mm^2
Park '03	2.2	2.3	75.0%	65.55mm^2
Nakazawa '00	3.0	0.96	81.9%	16 mm^2
Sato '00	5.0	0.36	82.0%	36 mm^2
Prabhakaran '05	5.0	0.01	78.0%	9.02 mm^2
O'Donnell '08	20.0	0.1	67.0%	6.4 mm^2

With such high frequencies the value of inductance needed is quite low (<200 nH), which may allow the possible integration of the inductor with the converter IC. The eventual aim of significantly increasing the switching frequency would be the achievement of the complete power-supply-on-chip (PwrSoC). However, an intermediate step toward this is the integration of the passives in package with the active components, i.e., a power-supply-in-package (PSiP). It should also be noted that several recent dc/dc converter products have included integration of the inductor into the same package as the active components. Notable steps toward monolithic integration include the work of Nakazawa *et al*. [4], which reported a converter IC with a monolithically integrated magnetic-core inductor, switching at 3 MHz and with a size of 16 mm^2. However, this inductor was still relatively large due to the significant inductance value (0.96 μH) required for the frequency of 3 MHz. Significant size reduction can be achieved by increasing the switching frequency further, and recently, Bergveld *et al*. [3] integrated a 1.3 mm × 1.3 mm, 20-nH air-core inductor and a 75-nF capacitor on the same die, to which they flip-chip attached the active component die, so enabling a system-in-package (SiP) application. This converter was demonstrated with a range of switching frequencies up to 100 MHz.

The use of magnetic-core inductors, as opposed to coreless inductors, has the advantages of increased inductance per unit area and containment of magnetic fields, with the disadvantages of extra loss incurred in the magnetic core, especially as the frequency is increased. Current state of the art for magnetic microinductors, as tested in dc/dc converter applications, is given in Table I [4]–[11].

In general, the lower switching frequency of most of the converters reported to date has required relatively large inductances, and hence inductors of relatively large size. Exceptions to this are the work of Prabhakaran *et al*. who demonstrated the use of

four 2.6-nH inductors in series in a converter at 5 MHz [11]. The total inductance was still only 10.4 nH and the converter achieved a 78% efficiency, excluding the gate-drive losses. Also, the output current of the converter at 5 A is quite high and would require a smaller inductance than most low-power switching converters. The work by O'Donnell *et al*. [5] demonstrates a relatively small (6.4 mm^2) microinductor in operation in a 20-MHz converter. The maximum efficiency of the microinductor in the converter in this case was estimated to be approximately 93%.

In general, if microinductors are to be successfully integrated in dc/dc converters then their size must be small and comparable to the size of the active components, and consequently, they must be capable of operation at high frequencies. Moreover, as standard discrete inductors provide the benchmark for inductor performance, it is important to understand the performance of the microinductor in comparison with discrete inductors. This paper investigates the operation of a microinductor in a 20–100 MHz dc/dc buck converter. We also compare the performance of the fabricated inductor to commercially available wirewound magnetic-core and air-core inductors. The microinductor device design and fabrication are described in Section II. Inductor performance characteristics are described in Section III. Section IV highlights measurement results for the microinductor and discrete inductors when used with a prototype high-frequency dc/dc down-converter IC. Conclusions and future developments are presented in Section V.

II. Device Design and Fabrication

There are several figures-of-merit (FoM) that can be used to define the performance of an inductor. These include the quality factor, the inductance enhancement achieved by the core, and the inductance-to-dc-resistance ratio. For an inductor used in a dc/dc converter, none of these are entirely satisfactory. For example, the quality factor gives the ratio of inductive impedance to ac resistance, but gives no indication of dc loss. This is similar for the inductance enhancement or inductance per unit area. The inductance-to-dc-resistance ratio is an important consideration for power inductors, but alone it does not give an indication of ac loss. In order to design the microinductor for dc/dc-converter operation, we therefore choose inductor efficiency defined as

$$\eta_{\text{ind}} = \frac{P_{\text{out}}}{P_{\text{out}} + P_{\text{ind}}}$$

where P_{out} is the converter output power and P_{ind} is the total inductor loss, as the FoM to maximize. The objective of the inductor design is, therefore, to maximize inductor efficiency with a given footprint area and with given technology parameters. The inductor loss includes winding and core loss, evaluated for the inductor current waveform, which will be encountered in the converter for the given converter operating conditions.

The inductor structure used is the traditional racetrack design with a magnetic core, as shown in Fig. 1. The coil consists of electroplated copper, which can be deposited to a maximum thickness of 50 μm. The magnetic material used is $Ni_{45}Fe_{55}$ alloy, which has a resistivity of 45 $\mu\Omega$/cm. The thickness of the layer of magnetic material is determined by the design, and is generally limited to less than 10 μm due to considerations of limiting the eddy current loss.

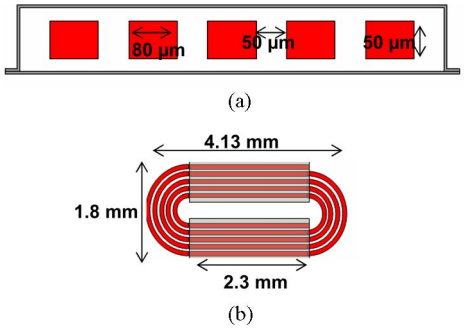

Fig. 1. (a) Cross section and (b) plan view of microinductor used in study.

TABLE II
Converter and Inductor Technology Parameters

Converter Specification	Values
Input Voltage	1.8 V
Output Voltage	1.12 V
Operating Frequency, MHz	20 – 100 MHz
Load Current	10 – 100 mA
Inductor Specifications	
No. of Turns	5
Area	7.48 mm^2
Winding Width	80 µm
Spacing	50 µm
Winding thickness	50 µm
Core Length	2.3 mm
Core Thickness	4.2 µm
Device Length	4.13 mm
Device Width	1.8 mm
Device Profile	0.17 mm

In previous work, the authors have developed an analytical model to design the microinductors [12]. This model can accurately predict the inductance, winding loss, and eddy and hysteresis loss of the magnetic material, given the inductor geometry and material parameters. This model is implemented in an optimization routine that varies the inductor geometrical parameters so as to maximize inductor efficiency for the given converter specifications. A range of inductors were designed using this approach for the general converter specifications given in Table II later.

The microfabricated inductor consists of a single layer of racetrack-shaped copper winding (five turns) sandwiched between two layers of magnetic material deposited by electroplating. The details of the inductor fabrication process have been previously described in [12]. From the range of inductors designed and fabricated a 150-nH inductor was chosen for testing with the converter, because it displayed the best L/R ratio for

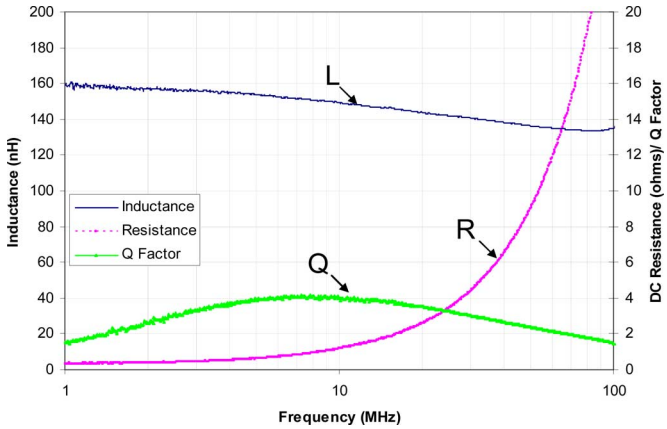

Fig. 2. Measured inductance (in henries), resistance (in ohms), and Q-factor versus frequency (in megahertzs) for the fabricated microinductor.

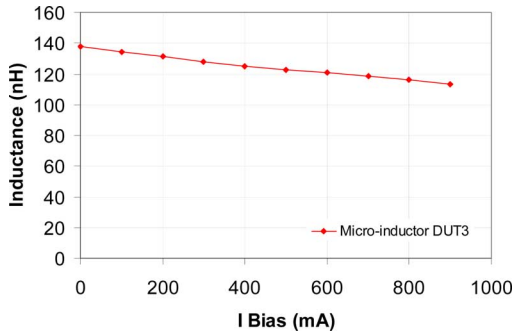

Fig. 3. Measured inductance of microinductor (in nanohenries) versus bias current (in milliamperes).

the range of fabricated devices. The dimensions of this inductor are also given in Table II.

The IC-fabrication-compatible process developed by the authors here allows fabricating inductors onto the same substrate or even directly on top of the power management IC to realize a truly monolithic dc/dc converter without the need for post-processing packaging.

III. Inductor Characteristics

After fabrication, the small-signal characteristics of the inductor were measured using the R&S Vector Network Analyzer, ZRVE. In order to do these measurements, the inductor was connected to a substrate with high-frequency coaxial connectors using wire bonds. The resistance and inductance were measured from 1 to 100 MHz. Note that this measurement includes the effect of the wire bond and substrate interconnect. A separate measurement of the wire bond and interconnect showed that these connections have an inductance of 10–15 nH and a resistance of approximately 250 mΩ. In the tests with the converter, wire bonding is also used to connect the inductor; thus, including the wire-bond resistance and inductance gives a realistic picture of the inductance and resistance seen in the converter. The measured inductance, resistance, and quality factor are shown in Fig. 2. The inductance characteristic from the graph has a relatively flat frequency response up to 30 MHz. The measured inductance at 10 MHz is approximately 150 nH and the measured resistance is 1 Ω.

When used in the converter, the inductor current waveform will have a dc component. It is therefore important to measure the inductance-versus-dc-bias-current characteristic for the inductors to determine the dc-handling capability. The current-handling ability of the inductor has been measured at 20 MHz using a HP 4285A LCR Meter with an HP 42841A current source. The dc-bias characteristic shows a small reduction in inductance up to 0.5 A. Note that in this case the inductance is less than obtained with the network-analyzer measurement because the device is measured directly without wire bonds, due to the low current-handling capability of the wire bonds. As the tests in the converter in this study are at an output current of approximately 70 mA, saturation of the microinductor should not be an issue.

IV. Performance in 20- to 100-MHz Buck Converter

Next, the microinductor has been tested in a high-frequency converter with switching frequencies from 20 to 100 MHz. The dc/dc buck converter was manufactured at NXP in a 0.18-μm CMOS process and converts an input voltage of 1.8 V down to an output voltage that is programmable between 0 and 1.8 V through a 6-bit digital duty-cycle code. For analysis purposes, the switching frequency has been made externally programmable through a variable resistor on the printed circuit board (PCB). A simple form of zero-voltage switching (ZVS) has been implemented to reduce switching losses. More details of this converter have been described in [3]. In fact, the converter IC used in this paper only contains the active die including power switches, drivers, and pulsewidth modulator (PWM). The same active die was also used in an SiP with the *LC* filter integrated in a passive die, as described in [3]. The optimum output current is 70 mA for ZVS operation, and this is the output current setting that we use in the comparison. The optimum current in ZVS operation depends on the switching frequency used. Bergveld *et al*. [3] found that an optimum current of 70 mA holds at a frequency of 100 MHz for a 20-nH inductor, which results in a rather large ripple current. For a larger inductance, as considered in this paper, the optimum current decreases at the same frequency. So, for 100 MHz, the optimum output current would drop to values below 70 mA. If the inductance can be increased by a factor of 7, the frequency can be decreased with roughly the same factor giving roughly the same optimum current. In our case, this suggests that for the 150-nH microinductor, the optimum current of 70 mA is valid at the lowest frequency, i.e., 20 MHz.

In order to connect the inductor to the converter IC, a test PCB was designed to enable the high-frequency measurements of the converter and the microinductor, see Fig. 4. The inductor is connected to the PCB with a wire-bond connection.

The test PCB allows for the measurement of the inductor current, which can be used to determine its actual inductance in the converter, verify whether or not the converter is in ZVS operation and determine inductor efficiency. To measure inductor current a 1-Ω SMD sense resistor was placed directly next

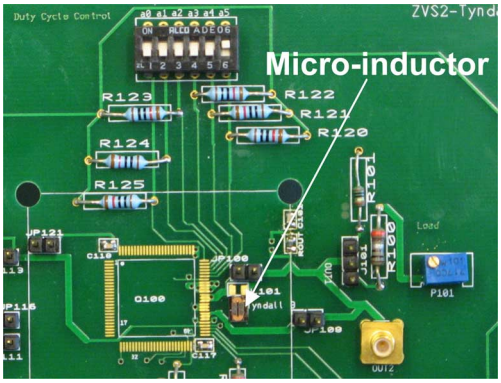

Fig. 4. Tyndall microinductor mounted on the ZVS buck-converter test PCB (IC not mounted on picture).

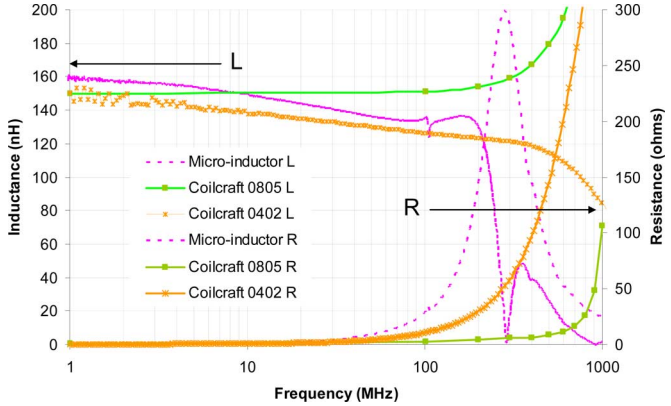

Fig. 5. Measured inductance (in henries) and resistance (in ohms) as a function of frequency (in hertzs) of the three inductor technologies in the comparison.

to the output filtering capacitor. The inductor current was measured differentially across the sense resistor using an FET probe and a digital oscilloscope. Single-ended voltage measurements at each side of the 1-Ω sense resistor were taken, stored, and subtracted for this purpose using the same trigger signal for both measurements. To verify the value of inductance of the microinductor in circuit, we calculate

$$V = L\frac{di}{dt}. \tag{1}$$

Taking the rising and the falling slopes of the inductor current, the inductance was measured to be 166 nH at 20 MHz in ZVS operation, which correlates quite closely to the design value of 150 nH.

As part of the tests, the performance of the fabricated inductor was compared to commercially available wire-wound chip inductors from Coilcraft. The chip inductors chosen for the comparison are a 0402AF-141 [13] 140-nH magnetic-core inductor and a 0805HS-151 [14] 150-nH air-core inductor. The 0402AF magnetic-core chip inductor is 0402 chip size (1.12 mm × 0.66 mm) and is 0.66 mm thick. The 0805HS air core is the standard 0805 chip size (2.16 mm × 1.52 mm) and is 1.45 mm thick.

Fig. 5 displays the measured inductance and resistance characteristics of the three technologies in the comparison. As we can see from the figure, the three inductors are relatively similar in inductance value up to 20 MHz. The air-core inductor has, however, a flatter inductance profile than either of the magnetic-core inductors indicating that the inductance contribution of the magnetic material decreases with frequency. The self-resonant frequency (SRF) of both the chip inductors is greater than 1 GHz, whereas for the microinductor the SRF is approximately 300 MHz, which indicates considerably higher parasitic capacitance in the case of the microinductor. The curves also show that the resistance of the microinductor increases faster with frequency. A review of the measured resistance and inductor areas for the three models in the comparison is given in Table III.

A. Measured Efficiencies of the Converter With the Inductor Technologies

The measured efficiencies of the ZVS buck converter with the three inductor technologies are shown in Fig. 6. Efficiency is measured at 70 mA output current and from 20 to 100 MHz. The converter input voltage was 1.8 V and the converter output voltage was approximately 1.12 V for the converter efficiency tests. The difference in converter maximum efficiency between using the commercially available chip inductors and the microinductor is approximately 2%. When using the microinductor, converter efficiency is approximately 78.5% at 20 MHz.

The efficiency measurements versus dc output current for the ZVS converter were taken from 10 to 100 mA at a 20 MHz switching frequency. Again, we compared the three different inductors by their performance in the converter. The input voltage for all measurements was 1.8 V, the duty cycle was fixed at 62%, and the output current was varied from 10 to 100 mA. Fig. 7 shows the obtained results. The microinductor performance again is slightly lower than the wire-wound inductors. Some of this is due to the effect of increased power loss from the added resistance of the wire bonds, which is analyzed in the next section.

B. Analysis of Converter Losses

Power loss for the converter can be divided into three main categories—switching, ohmic, and inductor loss, assuming other losses are negligible in ZVS operation. The total converter power loss is given by

$$P_{\text{loss\_converter}} = P_{\text{sw}} + P_{\Omega} + P_{\text{ind}}. \tag{2}$$

The switching loss is assumed to be entirely due to losses associated with parasitic capacitances, and hence can be expressed as

$$P_{\text{sw}} = fCV^2 \tag{3}$$

where V is the input voltage and C is an effective capacitance. The value of this effective capacitance can be determined by measuring the losses versus frequency at no load. To measure this switching loss of both power switches, P_{sw}, the load and *LC* filter were removed from the circuit and the input power was measured versus frequency. This input power is inclusive of the driver and PWM modulator power consumption. Losses due to dead time in ZVS operation are not included since the output current is zero, but are assumed to be small. The measurement

TABLE III
MEASURED RESISTANCE OF THREE INDUCTOR MODELS IN STUDY

Inductor	Area (mm^2)	R_{dc} (Ω)	R (Ω) at 20 MHz
Micro-inductor	7.48	0.191	3.5
Coilcraft 0805HS	2.5	0.560	0.780
Coilcraft 0402AF	0.5	0.260	1.45

was performed with the duty cycle set to 62% and $V_{\rm out}$ set to 1.12 V. From this measurement, the effective capacitance was estimated to be 90 pF.

The ohmic loss of the converter P_Ω was measured including the filter circuit, but subtracting the effect of the inductor resistance. The ohmic losses are given by

$$P_\Omega = I^2 R \tag{4}$$

where I is the current being drawn from the input supply source and R is the equivalent converter resistance, which is determined by plotting the imposed output current against the measured resulting output voltage of the converter. Since no internal control loop has been provided for on the IC, the output voltage will drop when the output current is increased. The equivalent converter resistance R can then be inferred from the slope of the resulting curve, after which the inductor resistance is subtracted. From this measurement, the equivalent resistance of the converter excluding the inductor was estimated to be 1.5 Ω. Once $P_{\rm sw}$ and P_Ω were evaluated, these values were added and the sum was subtracted from the total measured power loss. The resultant value is assumed to be the approximate measured power loss across the inductor $P_{\rm ind}$.

The overall measured converter loss, simulated inductor loss $P_{\rm ind}$, and total converter loss obtained by adding the simulated $P_{\rm ind}$ value to the ohmic loss P_Ω and switching loss $P_{\rm sw}$ inferred from measurements at a 20-MHz switching frequency for 10–100 mA output current is shown in Fig. 8. Equations (3) and (4) have been used to infer $P_{\rm sw}$ and P_Ω from the total measured losses, respectively. Microinductor loss $P_{\rm ind}$ was simulated using a frequency-dependent lumped equivalent circuit model of the inductor using a PSpice simulation of converter conditions for which the duty cycle was set to 62% and $V_{\rm out}$ was set to 1.12 V. At 20 MHz, it is evident that the switching and ohmic losses inferred from the measurements of the converter loss dominate at higher current when compared to inductor loss. In fact, the switching losses $P_{\rm sw}$ stay fixed with constant frequency, according to (3). However, the ohmic losses P_Ω increase with increasing output current,as given in (4).

From Fig. 8, it is evident that the measured overall converter power loss with both inductors is somewhat higher than the values obtained from (3) and (4) combined with simulated inductor loss. This is caused by dead-time losses, which are not taken into account in $P_{\rm sw}$ and P_Ω, but do occur in the measured overall losses.

Fig. 9 compares the inductor efficiencies inferred from measurements and those obtained from the inductor simulation for the ZVS converter with the microinductor and the Coilcraft 0402AF inductor. The converter operated again at 62% duty cycle and at an output current of 70 mA.

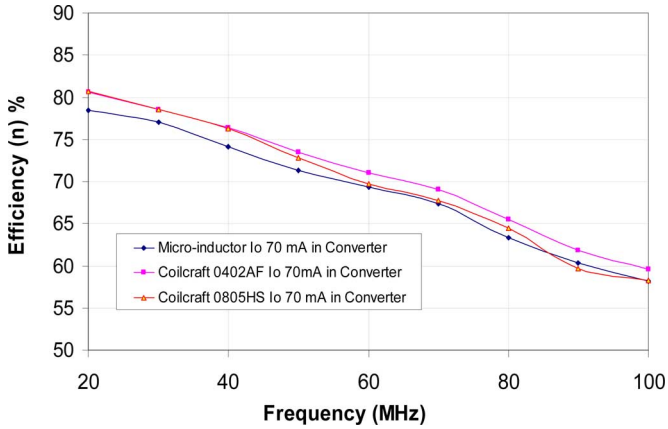

Fig. 6. Measured converter efficiency (in percentage) versus frequency (in megahertzs) for the three inductor technologies at 70 mA output current.

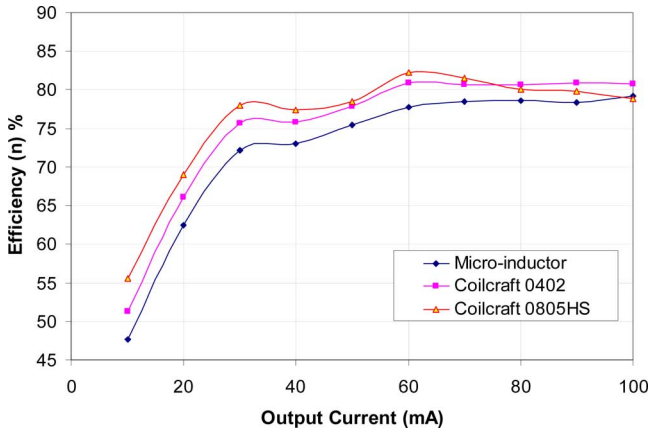

Fig. 7. Measured converter efficiency (in percentage) versus output current (in milliamperes) for the three inductor technologies at 20 MHz switching frequency.

The additional bond-wire effect of the microinductor adds additional dc resistance, and so reduces the overall converter efficiency. Fig. 9 also displays the improvement of the microinductor efficiency when the wire bonds are removed from the efficiency calculation. The inductor efficiency curves are consistent with the measured converter efficiency curves, in that the efficiency of the microinductor is shown to be 2%–3% lower than the chip inductors. The peak microinductor efficiency is approximately 93%, excluding the effects of the wire bonds.

For the microinductor, the loss can be examined in terms of the split between the winding loss (ac and dc) and the core loss. Fig. 10 shows a loss breakdown model of the microinductor for a load current of 100 mA, obtained from the inductor simulation model. This shows that the eddy current loss in the core material contributes 43% of the total losses of the microinductor.

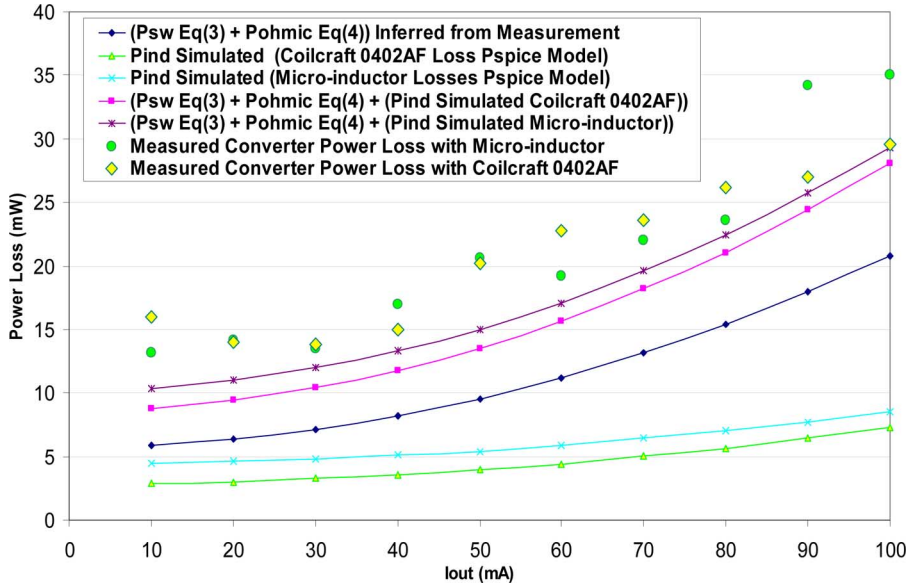

Fig. 8. Measured and simulated converter and inductor loss (in milliwatts) at 20 MHz switching frequency for 10–100 mA output current.

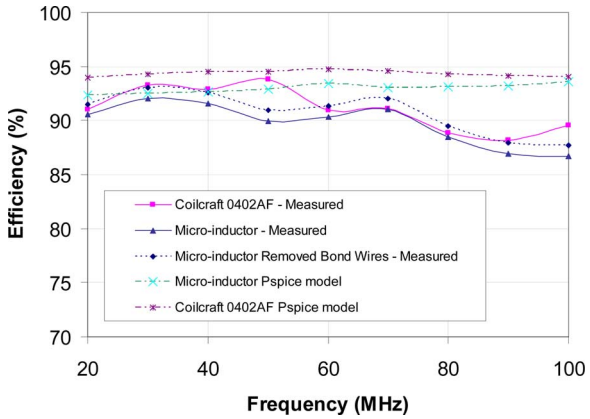

Fig. 9. Measured and simulated inductor efficiency of microinductor and Coilcraft chip inductor (in percentage) versus frequency (in megahertzs) when used in the ZVS buck converter.

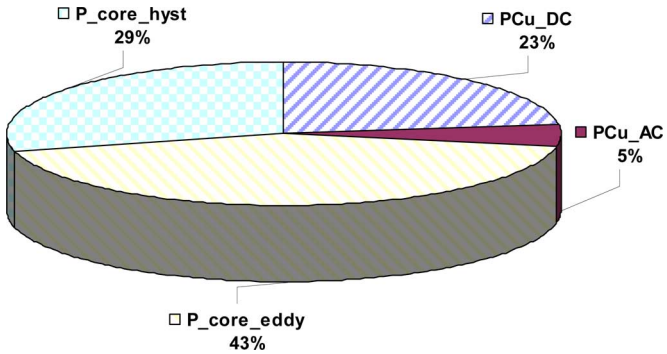

Fig. 10. Breakdown of losses in the microinductor for 100 mA dc output current and at a switching frequency of 20 MHz.

V. Conclusion

This paper has presented the design and measurement of a microinductor for use in a 20–100 MHz dc/dc converter. The microinductor has been shown to have a peak efficiency of 93% at 20 MHz and is approximately 2% less efficient than the equivalent magnetic and air-core chip inductor equivalents.

Even though microinductor efficiency is slightly below commercial chip alternatives, the difference in performance in the converter is small. From an analysis of the losses in a microinductor from 1 to 100 MHz, it is clear that both winding and core loss need to be further reduced. The winding loss is mainly due to the copper dc resistance and loss in the core is due to eddy current loss. The winding loss could be decreased by making the copper winding thicker and the core loss could be decreased by the addition of laminations to reduce the path area of circulating eddy currents [15].

With such a small difference in inductor performance from the study, one looks at the possible advantages of magnetic microinductors over chip alternatives. The profile of the microinductors is relatively low at 0.17 mm when compared to 1.45 mm of the 0805 air-core inductor and 0.66 mm of the 0402 magnetic-core inductor. This low profile may benefit packaging requirements to facilitate a complete SiP device. However, the microinductor still has quite a large area of 7.48 mm^2 compared to the smallest chip inductor that has an area of just 0.5 mm^2. If microinductor technology is to compete with chip inductors, device area must still be reduced substantially. Future microinductor devices will target a smaller surface area and an increased inductance per unit area. For future converter IC integration, low profile and small area of the microinductor will be necessary to facilitate a stacked-die solution or total integration on the silicon substrate. There is also the possibility to combine the microinductor technology with integrated-capacitor technology on a single die, which is beneficial when considering high-frequency dc/dc converters. Shorter high-frequency current loops would increase overall converter efficiency and reduce electromagnetic interference (EMI) problems, when compared to using external SMD passive devices.

ACKNOWLEDGMENT

The authors would like to thank L. Tiemeijer, R. Karadi, and K. Nowak of NXP Semiconductors for their contributions.

REFERENCES

[1] G. Schrom, P. Hazuchii, J. Hahn, D. S. Gardner, B. A. Bloechel, G. Dermer, S. G. Narendra, and T. Karnik, "A 480-MHz, multi-phase interleaved buck DC–DC converter with hysteretic control," in *Proc. IEEE Power Electron. Spec. Conf. (PESC'04)*, Aachen, Germany, Jun. 20–25, pp. 4702–4707.

[2] G. Schrom, P. Hazucha, F. Paillet, D. J. Rennie, S. T. Moon, D. S. Gardner, T. Kamik, P. Sun, T. T. Nguyen, M. J. Hill, K. Radhakrishnan, and T. Memioglu, "A 100-MHz eight-phase buck converter delivering 12A in 25mm^2 using air-core inductors," in *Proc. IEEE Appl. Power Electron. Conf. (APEC'07)*, Anaheim, CA, Feb. 25–Mar. 1, pp. 727–730.

[3] H. J. Bergveld, R. Karadi, and K. Nowak, "An inductive down converter system-in-package for integrated power management in battery-power applications," in *Proc. IEEE Power Electron. Spec. Conf. (PESC'08)*, Rhodes, Greece, Jun. 15–19, pp. 3335–3341.

[4] N. Nakazawa, M. Edo, Y. Katayama, M. Gekinozu, S. Sugahara, Z. Hayashi, K. Kuroki, E. Yonezawa, and K. Matsuzaki, "Micro DC/DC converter that integrates planar inductor on power IC," *IEEE Trans. Magn.*, vol. 36, no. 5, pp. 3518–3520, Sep. 2000.

[5] T. O'Donnell, N. Wang, R. Meere, F. Rhen, S. Roy, D. O'Sullivan, and C. O'Mathuna, "Microfabricated inductors for 20 MHz Dc–Dc converters," in *Proc. IEEE Appl. Power Electron. Conf. (APEC'08)*, Austin, TX, Feb. 24–28, pp. 689–693.

[6] T. Sato, K. Yamasawa, H. Tomita, T. Inoue, and T. Mizoguchi, "Planar power inductor using FeCoBN magnetic film with high saturation magnetization and high electrical resistivity," in *Proc. IEE Int. Power Electron. Conf. (IPEC'00)*, Tokyo, Japan, Apr. 3–7, pp. 303–308.

[7] C. S. Kim, S. Bae, H. J. Kim, S. E. Nam, and H. J. Kim, "Fabrication of high-frequency DC-DC converter using Ti/Fe TaN film inductor," *IEEE Trans. Magn.*, vol. 37, no. 4, pp. 2894–2896, Jul. 2001.

[8] K. H. Kim, J. Kim, H. J. Kim, S. H. Han, and H. J. Kim, "A megahertz switching DC/DC converter using FeBN thin film inductor," *IEEE Trans. Magn.*, vol. 38, no. 5, pp. 3162–3164, Sep. 2002.

[9] J. W. Park and M. G. Allen, "Ultralow-profile micromachined power inductors with highly laminated Ni/Fe cores: application to low-megahertz DC–DC converters," *IEEE Trans. Magn.*, vol. 39, no. 5, pp. 3184–3186, Sep. 2003.

[10] I. Kowase, T. Sato, K. Yamasawa, and Y. Miura, "A planar inductor using Mn-Zn ferrite/polyimide composite thick film for low-voltage and large-current DC–DC converter," *IEEE Trans. Magn.*, vol. 41, no. 10, pp. 3991–3993, Oct. 2005.

[11] S. Prabhakaran, Y. Sun, P. Dhagat, W. Li, and C. R. Sullivan, "Microfabricated V-groove power inductors for high-current low-voltage fast-transient DC–DC converters," in *Proc. IEEE Power Electron. Spec. Conf. (PESC'05)*, Recife, Brazil, Mar. 6–10, pp. 1513–1519.

[12] N. Wang, T. O'Donnell, S. Roy, P. McCloskey, and C. O'Mathuna, "Microinductors integrated on silicon for power supply on chip," *J. Magn. Magn. Mater.*, vol. 316, no. 2, pp. e233–e237, Sep. 2007.

[13] Coilcraft. (2007). Coilcraft Spice Model—0402AF, Document 558-1 [Online]. Available: http://www.coilcraft.com.

[14] Coilcraft. (2002). Coilcraft Spice Model—0805HS, Document 158-1 [Online]. Available: http: http://www.coilcraft.com.

[15] M. Brunet, T. O'Donnell, A. M. Connell, P. McCloskey, and S. C. O'Mathuna, "Electrochemical process for the lamination of magnetic cores in thin-film magnetic components," *J. Microelectromech. Syst.*, vol. 15, no. 1, pp. 94–100, Feb. 2006.

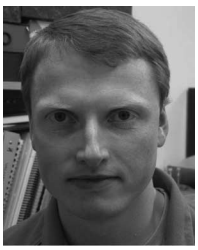

Ronan Meere (S'09) received the B.E. and M. Eng. Sc. degrees in electronic engineering from the National University of Ireland, Galway, Ireland, in 2003 and 2005, respectively. He is currently working toward the Ph.D. degree from the Microelectronic Engineering Department, Tyndall National Institute, University College Cork, Cork, Ireland.

His current research interests include the design and modeling of planar integrated magnetics for use in low-power-conversion applications.

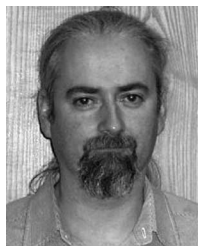

Terence O'Donnell (M'97) received the B.E. degree in electrical engineering from the University College, Dublin, Ireland, in 1990, and the Ph.D. degree from the National University of Ireland, Galway, Ireland, in 1996.

He is currently a Senior Research Officer with the Microsystems Research team in the Tyndall National Institute, Cork, Ireland. His current research interests include the design and modeling of planar and integrated magnetics for applications in power conversion and development of electromagnetic microgenerators for environmental and human body energy harvesting.

Henk Jan Bergveld was born in Enschede, the Netherlands, in 1970. He received the M.Sc. degree (*cum laude*) and the Ph.D. degree (*cum laude*) in electrical engineering from the University of Twente, Enschede, in 1994 and 2001, respectively.

In 1994, he joined Philips Research Laboratories, Eindhoven, the Netherlands. His previous research interests included modeling of rechargeable batteries to design better battery management systems. He has authored the book *Battery Management Systems—Design by Modeling* (Boston, MA: Kluwer, 2002). He was engaged in RFCMOS-integrated receivers and LCD column drivers, and since 2006, he has been involved in integrated dc/dc conversion. He is currently a Senior Principal leading a team of power-management experts with NXP Semiconductors, Eindhoven.

Ningning Wang received the Bachelor's and Master's degree in electrical engineering from Xi'an Jiaotong University, Xi'an, China, in 1995 and 1998, respectively, and the Ph.D degree in integrated magnetics for power conversion applications from the University College Cork, Cork, Ireland, in 2005.

In 2005, he joined the Tyndall National Institute, Cork, as a Postdoctoral Research Fellow and was appointed as a Staff Researcher in early 2008. He has extensive research experience in design, modeling, and fabrication of integrated magnetics for power conversion and data communications, and so far, he has authored or coauthored more than 30 papers in journals and peer-reviewed International Conference Proceedings. His current research interests include the design, modeling, and fabrication of integrated magnetic components, integrated capacitors, electromagnetic modeling and simulation, and development of electromagnetic microgenerators for environmental and human body energy harvesting.

Seán Cian O'Mathuna received the B.E., M.Eng.Sc., and Ph.D. degrees from the National University of Ireland, Cork, Ireland, in 1981, 1984, and 1994 respectively.

From 1982 to 1993, he was the Comanager of the Interconnection and Packaging Group, National Microelectronics Research Centre (NMRC), University College Cork, where he was a Senior Research Scientist. In 1993, he joined PEI Technologies, Naval Medical Research Center (NMRC), as the Technical/Commercial Director, where he was engaged in power packaging, planar/integrated magnetics, and product qualification. In 1997, he rejoined NMRC as a Group Director where he was involved in microsystems. In 1999, he was appointed as an Assistant Director for NMRC, where he was involved in microelectronics integration with research themes in ambient electronics biomedical microsystems, and energy processing for integrated circuit technology (ICT). He is currently a Director of the Tyndall National Institute, Cork, which incorporates NMRC and other research groups from University College Cork (UCC) and Cork Institute of Technology (CIT).